The Journal of Immunology, 2026, 215(5), vkag090
https://doi.org/10.1093/jimmun/vkag090
Cutting Edge

TGFβ primes alveolar-like macrophages to induce type I IFN following TLR2 activation

Sean M. Thomas[1], Abigail P. McGee[2,], Taryn E. Vielma[1,**], Laurisa M. Ankley[1,**], Alexander W. Rapp[2], Kayla N. Conner[1], Francois LeSage[2], Christopher Tanner[2], Eleanor C. Scheeres[1], Joshua J. Obar[2,*], and Andrew J. Olive[1,*]**

[1]Department of Microbiology, Genetics, and Immunology, College of Osteopathic Medicine, Michigan State University, East Lansing, MI, United States
[2]Department of Microbiology and Immunology, Geisel School of Medicine at Dartmouth, Lebanon, NH, United States
*Corresponding authors: Andrew J. Olive, Department of Microbiology, Genetics, and Immunology, Michigan State University, College of Osteopathic Medicine, East Lansing, MI 48824, United States. Email: oliveand@msu.edu and Joshua J. Obar, Department of Microbiology and Immunology, Geisel School of Medicine at Dartmouth, 1 Medical Center Drive, Lebanon, NH 03756, United States. Email: joshua.j.obar@dartmouth.edu
**These authors contributed equally.

Abstract

Alveolar macrophages (AMs) are key mediators of lung function and are potential targets for therapies during respiratory infections. TGFβ is an important regulator of AM differentiation and maintenance, but how TGFβ directly modulates the innate immune responses of AMs remains unclear. This shortcoming prevents effective targeting of AMs to improve lung function in health and disease. Here, we leveraged an optimized ex vivo AM model system, fetal liver–derived alveolar-like macrophages (FLAMs), to dissect the role of TGFβ in AMs. Using transcriptional analysis, we first globally defined how TGFβ regulates gene expression of resting FLAMs. We found that TGFβ maintains the baseline metabolic state of AMs by driving lipid metabolism through oxidative phosphorylation and restricting inflammation. To better understand inflammatory regulation in FLAMs, we next directly tested how TGFβ alters the response to TLR2 agonists. While both TGFβ (+) and TGFβ (−) FLAMs robustly responded to TLR2 agonists, we found an unexpected activation of type I interferon (IFN) responses in TGFβ (+) FLAMs and primary AMs. Surprisingly, mitochondrial antiviral signaling protein and the IFN regulator factors 3 and 7 were required for IFN production by TLR2 agonists and the IFN response was dependent on mitochondrial reactive oxygen species. Together, these data suggest that TGFβ modulates AM metabolic networks and innate immune signaling cascades to control inflammatory pathways in AMs.

Keywords alveolar macrophages, pulmonary innate immune responses, type I IFN regulation

Introduction

The pulmonary space is a specialized environment evolved to facilitate gas exchange and maintain lung function.[1,2] To protect against exposures to airborne microorganisms and particulates, lung alveoli contain a specialized phagocyte population, alveolar macrophages (AMs).[2,3] These AMs, like many other tissue-resident macrophages, seed the lungs from the fetal liver and serve two primary purposes: to preserve lung homeostasis by maintaining optimal surfactant levels in the lungs and to patrol the alveolar space for inhaled debris, initiating an inflammatory response when necessary.[4–6] Given the importance of maintaining pulmonary function, AMs must strictly regulate their inflammatory responses to prevent unnecessary inflammation and tissue damage.[7,8] Compared to other inflammatory macrophages, including bone marrow–derived macrophages (BMDMs), AMs are more hypoinflammatory against many pathogenic stimuli, a characteristic that is mediated by their distinct ontogeny and the lung environment.[8–10] In fact, circulating monocytes that are recruited to the lungs following infection have been shown to adapt to the local environment and take on AM-like phenotypes.[11] Two key cytokines, GM-CSF and TGFβ, are known to mediate AM differentiation and functions in the lung environment.[6,12–14] While the role of GM-CSF is better understood due to its importance in preventing pulmonary alveolar proteinosis, how TGFβ directly modulates the AM state and function remains unclear, limiting our ability to target AMs and improve lung function in health and disease.

TGFβ exists as three separate isoforms (TGFβ1–3) that all bind to the same TGFβ coreceptors (TGFβRI, TGFβRII).[15] TGFβ-1 is primarily produced by macrophages, but in an inactive form, conjugated with a latency-associated peptide (LAP).[16–18] Inactive TGFβ-1 (referred to as TGFβ from here on) is activated following enzymatic, acidic, or receptor-mediated cleavage of the LAP

Received: May 1, 2025. **Revised:** February 13, 2026. **Accepted:** February 18, 2026

from TGFβ.[18,19] In the lungs, inactive TGFβ is primarily produced by AMs, which is then activated by alveolar epithelial type II cells through the activity of the αvβ6 integrin on alveolar epithelial cells.[6,14,18] Thus, maintaining AMs requires unique interactions between the lung epithelium, and disruption of this environment results in dysregulated pulmonary responses.

In its active form, TGFβ is a versatile cytokine that triggers SMAD complex translocation to the nucleus to drive a multitude of processes, including stem cell differentiation, chemotaxis, and immune regulation, depending on the context in which it is acting.[20,21] Much of this heterogeneity in cellular responses to TGFβ is thought to be due to crosstalk between other transcriptional regulators and epigenetic regulation.[22] In the lungs, TGFβ plays critical roles both in lung development and disease. Mice lacking any of the three isoforms of TGFβ or either of the two receptors have varying degrees of deformed lung structure and alveologenesis due to dysregulated interactions between the lung epithelium and mesenchyme during development.[23–26] TGFβ is also implicated in the development of idiopathic pulmonary fibrosis through its induction of myofibroblast differentiation from lung fibroblasts and suppression of antifibrotic factors prostaglandin E2 and hepatocyte growth factor production.[27–29] Given the importance of TGFβ to maintain AMs in the lungs, it is essential to better understand how TGFβ modulates the inflammatory potential of AMs.

Fully dissecting the role of TGFβ in AM regulation requires ex vivo models that recapitulate key aspects of the lung environment. Recent work by several groups showed that growth of macrophages in both GM-CSF and TGFβ stabilizes the AM-like state for cells grown in culture.[30–32] We recently optimized the fetal liver–derived alveolar-like macrophage (FLAM) model, which propagates fetal liver cells in both GM-CSF and TGFβ, allowing for long-term propagation and genetic manipulation of cells that recapitulate many aspects of AM functions.[32] Removing TGFβ from these cells results in a loss of the AM-like state, such as decreased expression of the key AM transcription factor peroxisome-proliferating activating receptor gamma (PPARγ) and increased expression of the LPS co-receptor CD14. These data suggest that TGFβ not only maintains the AM state but also plays an important role in modulating the inflammatory response of AMs.

In this report, we directly examine how TGFβ shapes AM function and inflammatory responses. Using transcriptional analysis, we globally defined how TGFβ regulates the gene expression of resting FLAMs, identifying a key role of TGFβ in maintaining the metabolic state of AMs. In parallel, we characterized how TGFβ shapes the inflammatory response of AMs following the activation of Toll-like receptor 2 (TLR2), uncovering an unexpected link between TGFβ, TLR2, and type I interferon (IFN). We found that a range of TLR2 agonists activate type I IFN responses in a TGFβ-dependent manner. Further, mechanistic studies found this type I IFN response required the transcription factors interferon regulatory factors 3 and 7 (IRF3/7) in addition to the mitochondrial antiviral signaling adaptor (MAVS) protein. We also found increased peroxisome and mitochondrial organelle staining in response to TGFβ, resulting in increased reactive oxygen species (ROS) following TLR2 activation, which contributed to IFN production. Overall, these data suggest that TGFβ rewires the AMs and potentiates the activation of unique innate immune signaling not observed in other macrophage populations.

Materials and methods

Animals

Experimental protocols were approved by the Institutional Animal Care and Use Committees (IACUCs) at Michigan State University (MSU) (Animal Use Form no. PROTO202200127) and Dartmouth College (protocol #00002168). All protocols were strictly adhered to throughout the entire study. Six- to 8-week-old C57BL/6J mice (catalog no. 000664), *Tlr2*$^{(-/-)}$ mice (catalog no. 004650), and Cas9$^{(+)}$ mice (catalog no. 026179) were obtained from The Jackson Laboratory (Bar Harbor, ME, USA). Mice were given free access to food and water under controlled conditions (humidity, 40% to 55%; lighting, 12-hour light/12-hour dark cycles; and temperature, 24 ± 2 °C), as described previously.[32] Pregnant dams at 8 to 10 weeks of age and 14 to 18 gestational days were euthanized to obtain murine fetuses to generate FLAMs. Primary AMs and BMDMs were isolated from male and female mice >10 weeks of age.

FLAM cell culture

Wild-type (WT) and *Tlr2*$^{(-/-)}$ FLAMs were isolated as previously described.[32] In brief, pregnant dams were euthanized by CO_2 inhalation and secondary cervical dislocation. Fetuses were immediately removed, and loss of maternal blood supply served as a secondary form of death for the fetuses (MSU IACUC). Fetal livers were isolated and homogenized to single cell suspensions. These cells were then cultured in complete RPMI (Thermo Fisher Scientific) containing 10% FBS (R&D Systems), 1% penicillin-streptomycin (Thermo Fisher Scientific), 30 ng/mL recombinant mouse GM-CSF (PeproTech), and 20 ng/mL recombinant human TGFβ1 (PeproTech) included where indicated. FLAMs were selected by adherence on tissue culture plates following isolation. Media was refreshed every 2 to 3 days. When cells reached 70% to 90% confluency, they were lifted by incubating for 10 minutes with 37 °C PBS containing 10 mM EDTA, followed by gentle scraping.

AM and BMDM isolation and culture

Mice were euthanized by CO_2 exposure followed by exsanguination via the inferior vena cava. Lungs were lavaged as previously described.[32] This procedure has shown to not alter AM recovery or activation status[74] and does not impact the fetal liver cells isolated from neonates. Cells were then resuspended in RPMI 1640 media containing 30 ng/mL GM-CSF (PeproTech) and 20 ng/mL recombinant human TGFβ1 (PeproTech) and plated in untreated 48- or 24-well plates. AMs were lifted from plates using Accutase (BioLegend) and seeded for experiments.

For BMDMs, femurs were isolated and bone marrow was harvested following centrifugation of bones cut on one side. Bone marrow was then cultured in complete RPMI 1640 media containing 30 ng/mL M-CSF (PeproTech) for 7 days in untreated 15-cm dishes. Cells were then split for experiments and treated with or without 20 ng/mL recombinant human TGFβ1 (PeproTech) prior to activation.

Flow cytometry

To quantify surface expression of AM markers, cells were lifted by gentle scrapping, washed with PBS, and stained with SiglecF-Bv421

(BioLegend, catalog no. 155509), CD11b-APC (BioLegend, catalog no. 101212), CD14-PE-Cy7 (BioLegend, catalog no. 123316), and CD11a-PE (BioLegend, catalog no. 153103) (all diluted 1:400 in PBS). Cells were then washed 3 times in PBS and fixed with 1% formaldehyde (J.T. Baker, catalog no. JTB-2106-01) in PBS. The same gating strategy was used for all experiments and consists of live cells (Fixable Live/Dead Aqua BioLegend), forward scatter and side scatter, followed by doublet exclusion. Flow cytometry was performed on a BD LSR II or an Attune CytPix at the MSU Flow Cytometry Core, and data were analyzed using FlowJo (version 10.8.1).

TLR2 activation

Cells were seeded in 24-well or 48-well treated culture plates cells/well and allowed to settle overnight. Cells were treated with Pam3CSK4 25–200ng/mL (Invivogen, catalog no. tlrl-pms), peptidoglycan from *Staphylococcus aureus* at 50 μg/mL (Invivogen, catalog no. tlrl-pgns2), zymosan at 25–50 μg/mL or indicated concentrations (Invivogen, catalog no. tlrl-zyn), zymosan depleted at 50 μg/mL (Invivogen, catalog no. tlrl-zyd), and curdlan at 50 μg/mL (Invivogen, catalog no. tlrl-curd). As a control, direct TLR4 or TLR7 activation was mediated by LPS or R848 (Invivogen), respectively. RIG-I-like receptor (RLR) activation was mediated by treatment with 20 μg/mL Poly(I:C) (Invivogen, catalog no. tlrl-pic-5) complexed with Lyovec for transfection prior to stimulation.

Cytokine analysis

Where indicated, secreted CXCL10 and TNFα were quantified using the R&D Duoset kit (R&D Sciences) per manufacturer's instructions. Secreted IFNβ was quantified with the LumiKine Xpress mIFN-B 2.0 kit (Invivogen, catalog no. luex-mIFNβv2) per manufacturer's instructions. Luminescent signal was detected on a Spark multimode microplate reader (Tecan).

Lactate analysis

Intracellular levels of lactate were determined using an L-lactate assay kit (MilliporeSigma, catalog no. MAK329) according to manufacturer instructions.

Fluorescence microscopy staining and imaging

FLAMs grown with or without TGFβ were seeded 18 hours before immunofluorescence staining in glass-bottom MatTek dishes (MatTek P35G-1.5-14-C) and incubated under 2 mL of growth media overnight at 37 °C/5% CO_2. The following day, FLAM media was aspirated and washed with PBS, then fixed with prewarmed 4% paraformaldehyde for 20 minutes. Following PBS washes, FLAMs were permeabilized with 0.1% Triton X-100 and blocked with 10% newborn calf serum and 0.02% NaN_3. Cells were then incubated with primary antibody solution (10% newborn calf serum, 0.02% NaN_3, PBS, and primary Abs) for 90 minutes at room temperature with the following primary antibody concentrations: 14 μg/mL PMP70: Alexa Fluor 647 (Invitrogen, catalog no. PA1-650-A647), 10 μg/mL Catalase (R&D Systems, catalog no. AF3398), 4.5 μg/mL Tomm20 (Abcam, catalog no. AB78547), and 5 μg/mL ATP synthase (Invitrogen, catalog no. A21351). Following PBS washes, cell were incubated with secondary antibody solution (10% newborn calf serum, 0.02% NaN_3, 1× PBS, 2 μg/mL DAPI, and secondary Abs) for 1 hour in the dark at room temperature with the following 2° antibody concentrations: 30 μg/mL rabbit anti-goat IgG: FITC (Invitrogen, catalog no. 31509), 40 μg/mL goat anti-rat: Alexa Fluor 647 (Invitrogen, catalog no. A21247), and 40 μg/mL goat anti-mouse: fluorescein (Invitrogen, catalog no. F2761). Cells were then washed with PBS and stored in the dark until imaging.

For imaging analysis, asymmetric Z-stacks (step: 0.5 μm; below: −1.00 μm; above: 10.00 μm) of FLAMs were collected using a Nikon SoRa Spinning Disk Confocal Microscope and a Plan Apochromat Lambda D 100× Oil Immersion Objective Lens, N.A. 1.45. Images were processed using Fiji ImageJ.

ROS quantification and MitoTEMPO treatment

ROS were quantified using DCFDA-H2DCFDA staining according to kit protocol (Abcam; ab113851). In brief, FLAMs are incubated with 20 μM DCFDA-H2DCFDA for 30 minutes, then were treated with 50 μM tert-butyl hydroperoxide (TBHP) as a positive control for up to 4 hours at 37 °C. FLAMs were stimulated with 50 μg/mL zymosan for 4 hours or 100 ng/mL Pam3CSK4 for 1 hour prior to lifting and immediate flow cytometry analysis using a Cytek Aurora in the DartLab Flow Cytometry Core. To block mitochondrial ROS, at the time of activation, FLAMs were treated simultaneously with 500 μM MitoTEMPO (Sigma; SML0737), which remained in the media for the duration of the experiment. IFNβ was quantified from the supernatants by ELISA as described.

qRT-PCR

RNA from FLAMs was extracted using the Directzol RNA Extraction Kit (Zymo Research, catalog no. R2072) according to the manufacturer's protocol. Quality was assessed using NanoDrop. The One-step Syber Green RT-PCR Kit (Qiagen, catalog no. 210215) reagents were used to amplify the RNA and amplifications were monitored using the QuantStudio3 (Thermo Fisher, catalog no. A28567).

Pparg forward: TCGCTGATGCACTGCCTATG; *Pparg* reverse: GAGAGGTCCACAGAGCTGATT. *Gapdh* forward: AGGTCGGTGTGAA CGGATTTG; *Gapdh* reverse: TGTAGACCATGTAGTTGAGGTCA.

CRISPR-targeted knockouts

Lentiviral-mediated

Single-guide RNA (sgRNA) cloning sgOpti was a gift from Eric Lander and David Sabatini (Addgene plasmid no. 85681).[75] Individual sgRNAs were cloned as previously described.[76] In short, sgRNA targeting sequences (*Irf7*: TGTGCGGCCCTTGTACATGA; *Mavs*: GAGGACAAACCTCTTGTCTG; *Irf3*: GGCTGGACGAGAGCCGAACG) were annealed and phosphorylated, then cloned into a dephosphorylated and BsmBI (New England Biolabs) digested sgOpti. sgRNA constructs were then packaged into lentivirus as previously described and used to transduce early-passage $Cas9^+$ FLAMs. Two days later, transductants were selected with puromycin. After 1 week of selection, cells were validated for SiglecF/CD14 expression and used for experimentation.

Ribonuclear protein–mediated CRISPR editing

Three synthetic lyophilized sgRNAs (Synthego) per gene were pooled and prepared according to provided instructions. sgRNAs targeting *Mavs* and NLSx2-Cas9 protein were mixed with FLAMs in P2 primary cell nucleofection solution (Lonza, catalog no. V4XP-2024). Nucleofection was carried out using the 4D-Nucleofector Core and X Unit (Lonza, catalog no. AAF-1003B and AAF-1003X).

Mavs guide sequences: #1: AGGAAGCCCGCAGUCGAUCC; #2: UCUUCAAUAAUCUCCAGCGC; #3: UGCAGAUCUGUGAGCUGCCU.

Editing efficiency by inference of CRISPR edits analysis

Genomic DNA was isolated from control and target cells using the Qiagen DNeasy Blood and Tissue Kit (Qiagen, catalog no. 69506). Genomic DNA was quantified using a NanoDrop 1000 spectrophotometer (Thermo Scientific, catalog no. 2353-30-0010) and the edited region was amplified using PCR; the samples were then sequenced using Sanger sequencing (Genewiz) and editing efficiency was determined using inference of CRISPR edits analysis (Synthego).[77] All cells used have an efficiency >90%.

RNA sequencing analysis of naïve and activation FLAMs

FLAMs with and without TGFβ were plated in 6-well plates at 1×10^6 cells/well and treated with Pam3 as described above for 18 hours. We used the Direct-zol RNA Extraction Kit (Zymo Research, catalog no. R2072) to extract RNA according to the manufacturer's protocol. Quality was assessed by the MSU Genomics Core using an Agilent 4200 TapeStation System. The Illumina Stranded mRNA Library Prep kit (Illumina, catalog no. 20040534) with IDT for Illumina RNA Unique Dual Index adapters was used for library preparation following the manufacturer's recommendations but using half-volume reactions. Qubit dsDNA HS (Thermo Fisher Scientific, catalog no. Q32851) and Agilent 4200 TapeStation HS DNA1000 assays (Agilent, catalog no. 5067-5584) were used to measure quality and quantity of the generated libraries. The libraries were pooled in equimolar amounts, and the Invitrogen Collibri Quantification qPCR kit (Invitrogen, catalog no. A38524100) was used to quantify the pooled library. The pool was loaded onto 2 lanes of a NovaSeq S4 flow cell, and sequencing was performed in a 2×150-bp paired-end format using a NovaSeq 6000 v1.5 100-cycle reagent kit (Illumina, catalog no. 20028316). Base calling was performed with Illumina Real Time Analysis (RTA; version 3.4.4), and the output of RTA was demultiplexed and converted to the FastQ format with Illumina Bcl2fastq (version 2.20.0).

RNA sequencing (RNA-seq) analysis was completed using the MSU High Performance Computing Center. FastQC (version 0.11.7) was used to assess read quality. Bowtie2 (version 2.4.1)[78] with default settings was used to map reads with the GRCm39 mouse reference genome. Aligned reads counts were assessed using FeatureCounts from the Subread package (version 2.0.0).[79] Differential gene expression analysis was conducted using the DESeq2 package (version 1.36.0)[80] in R (version 4.2.1). All raw sequencing data, raw read counts, and normalized read counts are available through the National Center for Biotechnology Information's Gene Expression Omnibus database (accession no. GSE276577). Analyzed data in Table S1 are available on Figshare (https://doi.org/10.6084/m9.figshare.28914437).

Core AM upregulated signature genes were compared between FLAMs grown with and without TGFβ from our study and AMs and peritoneal macrophages from ImmGen (GSE122108[6,36]). Raw counts were compiled and normalized in DESeq2. A box plot was generated in GraphPad Prism using normalized counts for core AM upregulated signature genes. Gene set enrichment analysis (GSEA) was used to identify enriched pathways in the RNA-seq dataset. Genes in the indicated comparisons were ranked using DeSeq2, and the "GSEA preranked" function was used to complete functional enrichment using default settings for hallmark pathways from mice. We acknowledge our use of the GSEA, GSEA software, and Molecular Signature Database (MSigDB)[59] (http://www.broad.mit.edu/gsea/).

Results

TGFβ drives lipid metabolism, restrains cytokine expression, and maintains FLAMs in the AM-like state

We previously developed FLAMs as an ex vivo model of AMs to understand the mechanistic signals and regulatory networks that maintain cells in the AM-like state.[32] For this model, the source of pulmonary AMs, the fetal liver, is removed from neonates and cells are cultured in media containing both GM-CSF and TGFβ. This model enables rapid isolation, growth, and cryopreservation of nonimmortalized AM-like cells. In this model, TGFβ—a key cytokine needed to maintain AMs in vivo—is needed to maintain FLAMs in the AM-like state, yet how TGFβ modulates AM functions and transcriptional networks remains poorly resolved.[6,14,32] As a first step, we confirmed that TGFβ is required to broadly maintain the AM-like state in FLAMs. FLAMs were grown in medium containing GM-CSF with or without TGFβ for 2 weeks and the expression of the AM-associated surface markers SiglecF (high) and CD14 (low) was quantified by flow cytometry. We observed that FLAMs grown with TGFβ had high expression of SiglecF and CD11a together with low expression of CD14 and CD11b on their surface, while FLAMs grown without TGFβ had the opposite pattern of expression with low expression of SiglecF and CD11a and higher expression of CD14 and CD11b (Fig. 1A). Since PPARγ is a key transcription factor in AMs and is expressed in both AMs and FLAMs,[32,33] we measured the effect of TGFβ on PPARγ expression. mRNA was isolated from FLAMs grown with and without TGFβ and quantitative RT-PCR was used to determine the expression of *Pparg*. FLAMs grown with TGFβ maintained higher expression of *Pparg*, while cells grown in the absence of TGFβ showed significantly decreased *Pparg* expression (Fig. 1B). These data confirm that TGFβ helps maintain FLAMs in an AM-like state, similar to what has been seen with TGFβ's role in differentiation and maintenance of AMs in the lungs.[6,32]

To better understand how TGFβ globally regulates FLAMs, we next conducted whole-transcriptome RNA-seq analysis on FLAMs grown in the presence and absence of TGFβ. Differential expression analysis identified hundreds of genes that were significantly changed between FLAMs grown with or without TGFβ

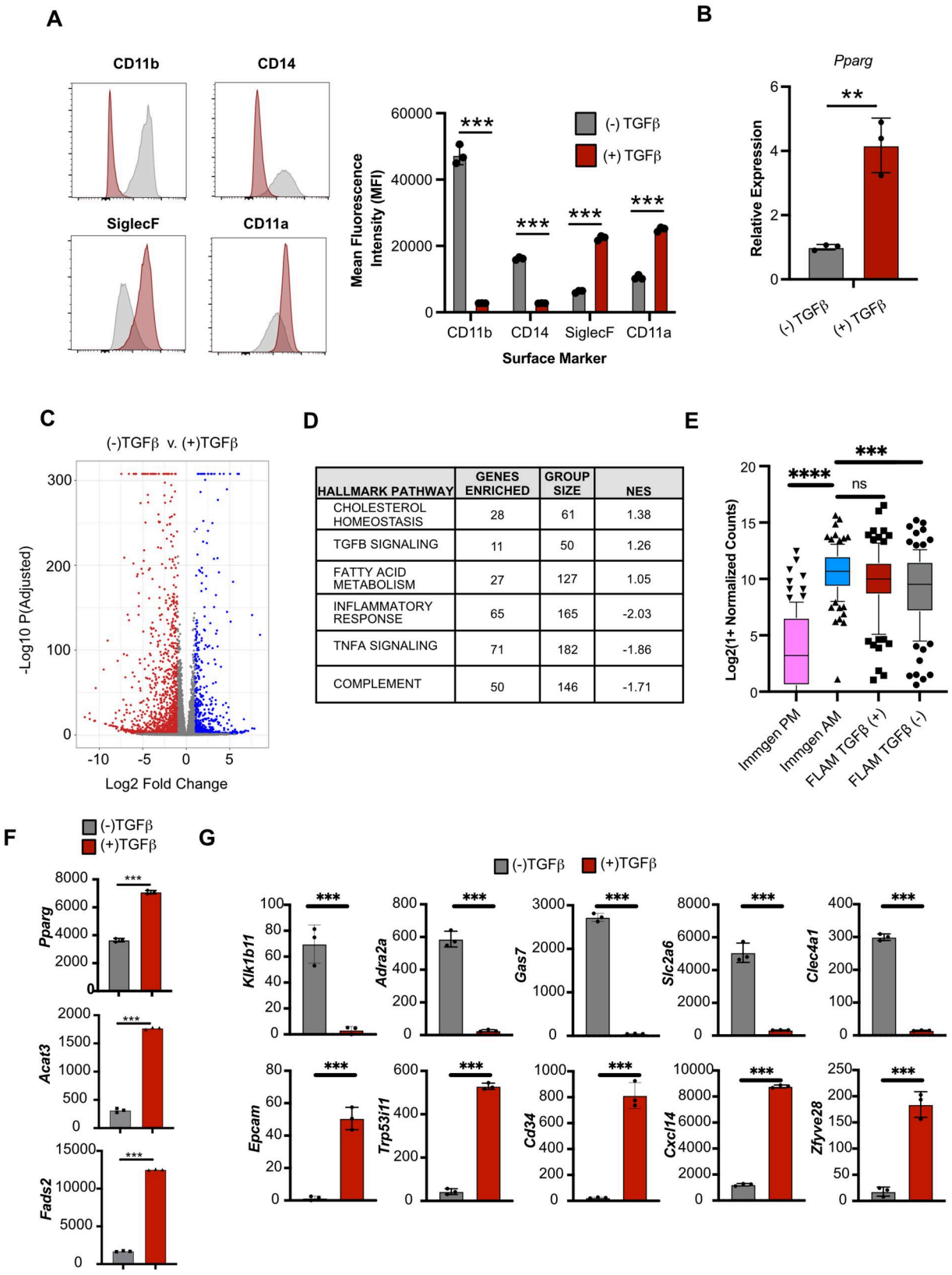

HALLMARK PATHWAY	GENES ENRICHED	GROUP SIZE	NES
CHOLESTEROL HOMEOSTASIS	28	61	1.38
TGFB SIGNALING	11	50	1.26
FATTY ACID METABOLISM	27	127	1.05
INFLAMMATORY RESPONSE	65	165	-2.03
TNFA SIGNALING	71	182	-1.86
COMPLEMENT	50	146	-1.71

Figure 1. TGFβ drives lipid metabolism, restrains chemokine expression, and maintains FLAMs in the AM-like state. (A) The expression of the indicated surface markers was quantified by flow cytometry from TGFβ (+) and TGFβ (−) FLAMs and are shown as representative histograms (left) and the quantified MFI (right). Each point represents a technical replicate from 1 of 3 representative experiments. $^{**}P < 0.01$ by unpaired Student t-test. (B) *Pparg* expression was quantified by qRT-PCR using $2^{(-\Delta\Delta CT)}$ relative to GAPDH in untreated TGFβ (+) and TGFβ (−) FLAMs. Each point represents a technical replicate from 1 representative experiment of 3. $^{**}P < 0.01$ by unpaired Student t-test. (C) Differentially expressed genes were

Figure 1. Continued
identified between untreated TGFβ (+) and TGFβ (−) FLAMs. Red points represent significantly underexpressed genes (adjusted $P < 0.05$) and blue points represent significantly overexpressed genes (adjusted $P < 0.05$) between TGFβ (+) and TGFβ (−) FLAMs. Each point represents the mean of 3 biological replicates from 1 experiment. DESeq2 was used to determine significance using the adjusted P value to account for multiple hypothesis testing. (D) Shown are the top hallmark pathways enriched in TGFβ (+) and TGFβ (−) FLAMs. (E) Normalized counts of core AM genes were compared among TGFβ (+) and TGFβ (−) FLAMs and previously published datasets from ImmGen (ImmGen PM and ImmGen AM; accession no. GSE122108, https://www.ncbi.nlm.nih.gov/geo/query/acc.cgi? acc=GSE122108). The box plot shows the median with quartiles representing the 10th to 90th percentile range of the data within that cell type. Each point represents the mean normalized counts of an individual gene. The Mann–Whitney U test was used to make statistical comparisons between each cell type and to compare medians (*** $P < 0.001$; **** $P < 0.0001$; ns, not significant) (F) Gene expression was quantified from normalized counts for key genes important in lipid metabolism. (G) Gene expression was quantified from normalized counts for a subset of genes differentially expressed from Yu et al.[6] For (F) and (G), each point represents a technical replicate from 1 experiment. ***Adjusted $P < 0.001$ using DeSeq2 analysis. NES, normalized enrichment score; ns, not significant.

(Fig. 1C and GSE276577 for normalized count table). To globally identify pathways that were uniquely enriched in TGFβ (+) FLAMs, we employed GSEA, using a ranked gene list generated from the differential expression analysis (Fig. 1D). Among the top hallmark pathways enriched in TGFβ (+) FLAMs were cholesterol homeostasis, TGFβ signaling, and fatty acid metabolism (Fig. 1D and Fig. S1A). Supporting this observation, TGFβ (+) FLAMs contained significantly less intracellular lactate than TGFβ (−) FLAMs (Fig. S1B). Given that AMs are known to drive PPARγ-dependent lipid metabolism, these data suggest that the FLAM transcriptional profile is similar to primary AMs.[34,35] In contrast, pathways enriched in TGFβ (−) FLAMs included the inflammatory response, TNFα signaling, and complement (Fig. 1D and Fig. S1A). To directly test similarities between FLAMs and primary AMs, we compared the expression of a previously published AM gene signature between our FLAMs grown with and without TGFβ in addition to primary AMs and peritoneal macrophages from the immunological genome project (ImmGen) (Fig. 1E and Table S1).[36] While there was no significant difference in the expression of this gene signature between primary AMs and TGFβ (+) FLAMs, there was a significant difference between primary AMs and TGFβ (−) FLAMs, supporting that TGFβ maintains FLAMs in an AM-like state. We next directly compared the expression of a subset of genes related to differentially expressed pathways (Fig. 1F). We found high expression of lipid metabolism genes, including *Pparg*, *Acat3*, and *Fads2* in TGFβ (+) FLAMs. These data support a key role of TGFβ in maintaining the AM-specific metabolic state. To examine the relevance of FLAMs as a model of primary AMs, we compared our transcriptomics with those identified from Yu and colleagues, who examined the transcriptome of sorted primary AMs with and without the TGFβR.[6] Of the top 15 genes that Yu et al. found to be upregulated or downregulated from AMs in the lungs, 13 of 15 upregulated and 12 of 15 downregulated genes were similarly differentially expressed significantly in TGFβ (+) and TGFβ (−) FLAMs (Fig. 1G and Table S1). These data strongly suggest that FLAMs recapitulate the biology observed in the lungs of intact animals and provide a useful tool to dissect the underlying mechanisms of TGFβ on primary AMs.

TGFβ mediates a type I IFN response in AMs following Pam3CSK4 activation

To understand how TGFβ alters the innate immune response of AMs, we next directly tested the response of FLAMs grown with and without TGFβ to inflammatory stimuli. Many bacterial and fungal respiratory pathogens activate TLR2 signaling during infection.[37–41] Thus, we examined whether the activation of TLR2 by the purified agonist Pam3CSK4 (referred to as Pam3) alters the transcriptome of FLAMs in a TGFβ-dependent manner. TGFβ (+) and TGFβ (−) FLAMs were stimulated with Pam3 for 18 hours, then RNA-seq and differential expression analysis were used to identify changes in the transcriptional landscape. We identified >700 genes that were significantly altered following Pam3 treatment of TGFβ (+) FLAMs compared to untreated TGFβ (+) FLAMs (Fig. S2A and GSE276577 for normalized counts). We were next curious which pathways were enriched among differentially expressed genes in TGFβ (+) FLAMs compared to TGFβ (−) FLAMs following Pam3 treatment to identify TGFβ-dependent and, perhaps, AM-specific immune signaling (Fig. 2A). Using GSEA hallmark pathways, we found continued enrichment of cholesterol homeostasis pathways in addition to a strong enrichment in E2F targets (Fig. S2B). Unexpected enrichment in IFNα response in the TGFβ (+) FLAMs (Fig. 2B). When we examined the entire IFNα hallmark pathway, which encompasses the general type I IFN response, across all conditions we only observed robust induction of IFN-related genes in Pam3-treated TGFβ (+) FLAMs (Fig. 2C). This finding suggests that TGFβ skews macrophage responses to drive the activation of type I IFN pathways following Pam3 stimulation.

To further understand the functional outcomes of TLR2 dimerization in TGFβ (+) FLAMs, we next directly examined the normalized reads of IFN-related genes. Our transcriptome data showed no expression of any *Ifna* gene or *Ifne* and *Ifng*, but we did observe increased expression of *Ifnb1* and the IFN-stimulated genes *Cxcl10* and *Rsad2* (Fig. 2D), suggesting that IFNβ is driving the gene signature. We observed similar baseline expression of *Ifnb1*, *Cxcl10*, and *Rsad2* between conditions; however, TGFβ (+) FLAMs induced significantly higher expression of all three genes following Pam3 treatment. To corroborate the RNA-seq results, we compared the secretion of cytokines in resting and Pam3-treated TGFβ (+) and TGFβ (−) FLAMs using an ELISA (Fig. 2E). In agreement with our transcriptional results, we observed a significant increase in IFNβ and CXCL10 secretion from Pam3-treated TGFβ (+) FLAMs compared to TGFβ (−) FLAMs. In line with our Pam3-simulated TGFβ (+) FLAMs, we observed that 2 additional agonists that mimic bacterial or fungal infection (peptidoglycan and zymosan, respectively) resulted in a significant increase in CXCL10 production in TGFβ (+) FLAMs compared to TGFβ (−) FLAMs (Fig. S2C). In contrast, we observed no significant CXCL10

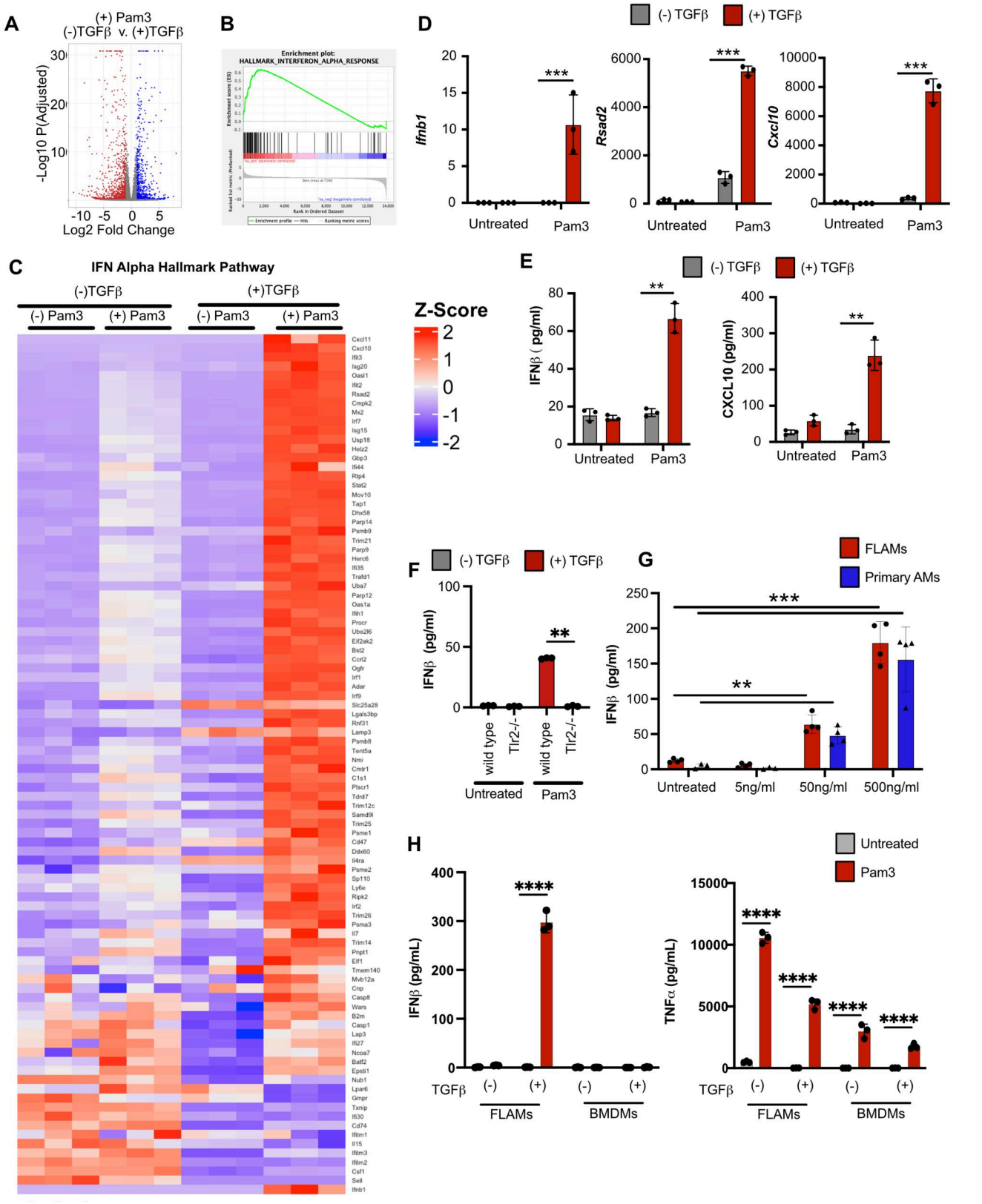

Figure 2. TGFβ mediates type I IFN responses during TLR2 activation. (A) TGFβ (+) and TGFβ (−) FLAMs were stimulated with 50 ng/mL Pam3, and 18 h later differentially expressed genes were identified between TGFβ (+) and TGFβ (−) FLAMs left untreated or treated with Pam3 for 18 h. Red points represent significantly underexpressed genes (adjusted $P < 0.05$) and blue points represent significantly overexpressed genes (adjusted $P < 0.05$) between TGFβ (+) and TGFβ (−) FLAMs. (B) Leading edge analysis of differentially expressed genes identified the IFNα response hallmark pathway comparing Pam3 activation in TGFβ (+) and TGFβ (−) FLAMs. (C) Expression of genes representing the IFNα hallmark pathway between TGFβ (+) and TGFβ (−)

secretion following activation with depleted zymosan or curdlan (Fig. S2C), which are pure dectin-1 ligands.[42] Importantly, this distinct IFN induction was not due to differential expression of TLR2 between TGFβ (+) FLAMs and TGFβ (−) FLAMs as we noted similar expression in the RNA-seq results and by flow cytometry (Fig. S2D).

Since our results suggested that TLR2 activation drives an increased type I IFN response in TGFβ (+) FLAMs, we first directly tested the role of TLR2 signaling in the induction of the type I IFN response using *Tlr2*$^{(-/-)}$ FLAMs. WT and *Tlr2*$^{(-/-)}$ TGFβ (+) FLAMs were stimulated with Pam3 and the IFNβ protein concentrations were quantified in the supernatants by ELISA the following day. While WT TGFβ (+) FLAMs robustly induced IFNβ, this was lost in *Tlr2*$^{(-/-)}$ FLAMs (Fig. 2F). This result suggests that TGFβ signaling in FLAMs drives a unique response to TLR2 activation that results in the production of type I IFN.

We next confirmed that this phenotype occurs in primary murine AMs by isolating cells from the lungs and treating them with increasing Pam3 concentrations, subsequently examining the production of IFNβ by ELISA (Fig. 2G). In line with our results in FLAMs, we observed a significant, dose-dependent increase in IFNβ in primary murine AMs following treatment with Pam3. To determine if this innate response was AM specific, we next examined primary BMDMs. FLAMs or BMDMs were grown with or without TGFβ then stimulated with Pam3, and the following day, IFNβ and TNFα were quantified by ELISA (Fig. 2H). While we observed TNFα production in all conditions, albeit to varying levels, we only observed increased IFNβ secretion from FLAMs grown in TGFβ. We next determined if this type I IFN response was specific to TLR2. TGFβ (+) FLAMs and TGFβ (−) FLAMs were left untreated or were treated with LPS, R848, or PolyI:C; then the levels of IFNβ were quantified 24 hours later (Fig. S2E, F). Similar to TLR2 activation, activation of each distinct pattern recognition receptor (PRR) drove a significant increase in IFNβ production in a TGFβ (+) dependent way. Taken together, these data suggest that TGFβ drives fetal liver–derived macrophages but not BMDMs to produce type I IFN in response to diverse PRR activation.

TLR2 signaling in TGFβ (+) FLAMs induces an RLR gene signature and type I IFN production is dependent on MAVS, IRF3, and IRF7

We next wanted to better understand the mechanisms driving the TLR2-dependent type I IFN response in TGFβ (+) FLAMs. When we examined the KEGG pathway enrichment in our transcriptional analysis in Pam3-treated TGFβ (+) and TGFβ (−) FLAMs, we observed a strong signature for RLR signaling (Fig. 3A and Fig. S3A). RLR signaling converges on the MAVS protein, which triggers the activation of the transcription factors interferon regulatory factors 3 and 7 (IRF3/IRF7) to mediate the transcription of IFNβ.[43,44] To test the role of these genes in controlling TGFβ-dependent type I IFN responses after Pam3 stimulation, we used our previously described CRISPR-Cas9 editing approaches in FLAMs to target *Mavs*, *Irf3*, and *Irf7* with individual sgRNAs.[32] We first confirmed the functional effects of editing by stimulating TGFβ (+) control, sgMAVS, sgIRF3, and sgIRF7 FLAMs with Poly(I:C) and measured IFNβ production by ELISA.[45] We observed a significant decrease in IFNβ for all three genes targeted, suggesting functional defects in RLR signaling (Fig. 3B). We next tested the response of these cells to Pam3 and zymosan. The following day, secreted IFNβ was quantified by ELISA. Similar to our previous findings, we observed that WT FLAMs induced IFNβ in response to both Pam3 and zymosan (Fig. 3C). Surprisingly, we found that IFNβ secretion after both Pam3 and zymosan treatment was significantly reduced from the sgMAVS, sgIRF3, and sgIRF7 FLAMs (Fig. 3C). These data suggest that TGFβ-dependent, TLR2-mediated type I IFN responses are controlled by MAVS and IRF3/IRF7. To account for possible effects of lentiviral transduction, we next used Cas9-mediated editing with ribonuclear protein (RNP) to generate *Mavs*-deficient FLAMs. These *Mavs*-deficient cells did not produce IFNβ in response to Poly(I:C), suggesting functional knockout of MAVS (Fig. 3D). In agreement with our lentiviral-delivered sgRNA studies, we found that genetic loss of *Mavs* results in a reduction in IFNβ following both Pam3 and zymosan stimulation (Fig. 3E). Thus, TGFβ-dependent, TLR2-mediated type I IFN responses are controlled by MAVS-dependent signaling.

Mitochondrial oxidative stress contributes to TLR2-dependent IFNβ production

Given MAVS was required for the type I IFN response, we next wanted to understand the mechanisms driving MAVS activation and signaling. Our transcriptomics suggest that TGFβ drives lipid metabolism, and the cellular hubs of lipid metabolism—peroxisomes and mitochondria—are known to activate type I IFN responses.[46,47] Thus, we hypothesized that TGFβ-dependent changes to peroxisomes and mitochondria levels and/or function may condition FLAMs to drive MAVS-dependent IFNβ

Figure 2. Continued
FLAMs that have or have not been treated with Pam3. Each column of 3 biological replicates represents an experimental condition from 1 experiment. (D) Normalized read counts from *Ifnb*, *Rsad2*, and *Cxcl10* from Pam3 RNA-seq experiment. ***Adjusted $P < 0.001$ using DeSeq2 analysis. (E) TGFβ (+) and TGFβ (−) FLAMs were stimulated with Pam3 for 24 h. Supernatants were collected for quantification of IFNβ and CXCL10 by ELISA. (F) TGFβ (+) FLAMs or primary AMs from C57BL6/J mice were stimulated with the indicated concentrations of Pam3, and IFNβ was quantified by ELISA the following day. Shown is 1 representative experiment of 3 each containing 3 replicates per experiment. **$P < 0.01$, ***$P < 0.001$ by 1-way ANOVA with a Tukey post hoc test for multiple comparisons. (G) WT FLAMs or *Tlr2*$^{(-/-)}$ FLAMs were stimulated with Pam3 for 24 h. Secreted IFNβ was quantified by ELISA. Each point represents data from a single well from 1 of 3 representative experiments. **$P < 0.01$, ****$P < 0.0001$ by 1-way ANOVA with a Tukey post hoc test for multiple comparisons. (H) FLAMs or BMDMs grown with or without TGFβ were stimulated with Pam3 for 24 h, and IFNβ (left) and TNF (right) were quantified by ELISA. Shown is 1 of 4 representative experiments containing 3 replicates per group.

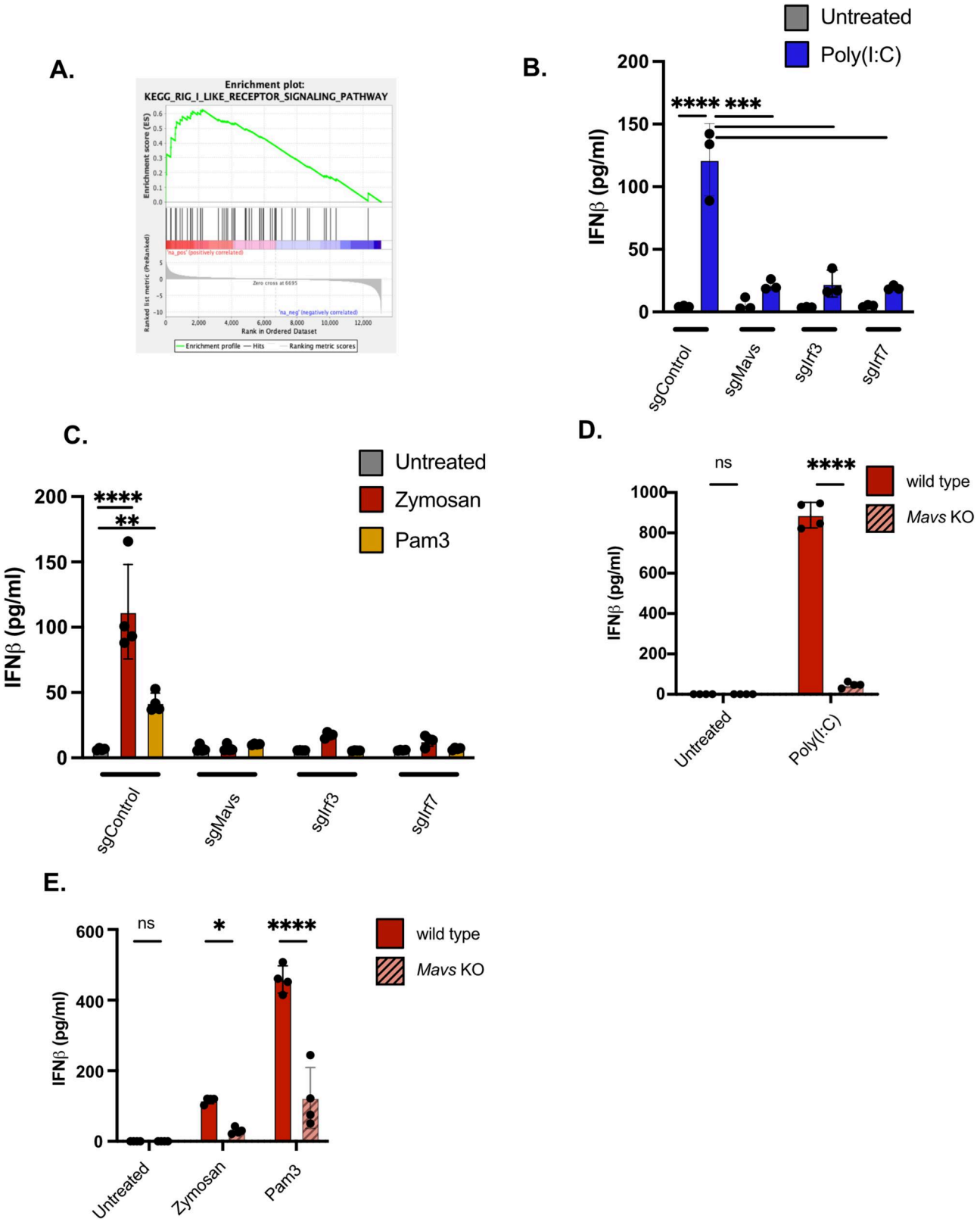

Figure 3. MAVS contributes to TGFβ-dependent type I IFN responses. (A) Leading edge analysis of differentially expressed genes identified RLR signaling comparing Pam3 activation in TGFβ (+) and TGFβ (−) FLAMs. (B) WT, sgMAVS, sgIRF3, and sgIRF7 FLAMs were stimulated with Poly(I:C) for 24 h. Secreted IFNβ was quantified by ELISA. Shown is a representative experiment of 3 with at least 3 samples per group. (C) WT, sgMAVS, sgIRF3, and sgIRF7 FLAMs were stimulated with Pam3 or zymosan (1 μg/mL) for 24 h. Secreted IFNβ was quantified by ELISA. Shown is a representative experiment of 3 with at least 3 samples per group. (D) WT or *Mavs* KO FLAMs were stimulated with Poly(I:C) for 24 h. Secreted IFNβ was quantified by ELISA. (E) WT or *Mavs* KO TGFβ (+) FLAMs were stimulated with Pam3 or zymosan (1 μg/mL) for 24 h. Secreted IFNβ was quantified by ELISA. Each point represents data from a single well from 1 of 4 representative experiments. *$P<0.05$,**$P<0.01$, ***$P<0.001$, *$P<0.0001$ by 1-way ANOVA with a Tukey post hoc test for multiple comparisons. ns, not significant.

secretion following TLR2 activation. To test this hypothesis, we first examined peroxisomes and mitochondria in resting cells by immunofluorescent staining coupled with quantifying the mean fluorescence intensity (MFI) in WT TGFβ (−) FLAMs in addition to WT and *Mavs* knockout (KO) TGFβ (+) FLAMs. To visualize the presence of peroxisomes, we examined both PMP70, a peroxisome membrane–associated protein and catalase, a luminal peroxisome enzyme (Fig. 4A). We observed a significant increase in the MFI of both markers in WT TGFβ (+) FLAMs compared to TGFβ (−) FLAMs (Fig. 4B). Similarly, we noted a marked increase in PMP70 and catalase staining in freshly isolated primary AMs obtained via bronchoalveolar lavage when compared to BMDM (Fig. S4A). We also noted that *Mavs* KO FLAMs resulted in a significant decrease in the MFI of peroxisomal markers, which was more like the TGFβ (−) FLAMs. We next repeated this experiment using the mitochondrial markers Tomm20 and ATP synthase (Fig. 4C). We found that WT TGFβ (+) FLAMs had a 2-fold increase in the Tomm20 MFI and a 5-fold increase in the MFI of ATP synthase compared to TGFβ (−) FLAMs (Fig. 4D). Again, freshly isolated primary AMs had significantly greater Tomm20 and ATP synthase staining compared to BMDM (Fig. S4B). In contrast, we found that *Mavs* KO TGFβ (+) FLAMs showed a similar increased staining of Tomm20 compared to WT TGFβ (+) FLAMs but showed a reduction in ATP synthase staining. These data suggest that peroxisome and mitochondrial numbers are increased in TGFβ (+) FLAMs prior to activation and these organelles may be altered by the loss of MAVS.

Since lipid metabolism is a robust source of ROS, we next hypothesized that increased peroxisome and mitochondria levels would result in increased ROS, which could enhance MAVS-dependent signaling.[48,49] To begin to test this hypothesis, we initially quantified total ROS in cells using the fluorescent dye DCFDA-H2DCFDA in WT TGFβ (−) FLAMs in addition to WT and *Mavs* KO TGFβ (+) FLAMs following activation with Pam3 or zymosan (Fig. 4E). We observed an approximate 3-fold increase in the DCFDA-H2DCFDA MFI in WT TGFβ (+) FLAMs following activation with either Pam3 or zymosan compared to WT TGFβ (−) FLAMs and *Mavs* KO TGFβ (+) FLAMs. These data suggest a significant increase of ROS in TGFβ (+) FLAMs following TLR2 activation. To understand the functional consequences of increased ROS, we next blocked mitochondrial-derived ROS with treatment of the mitochondrial-specific antioxidant MitoTEMPO.[50] Both WT TGFβ (+) and TGFβ (−) FLAMs were stimulated with Pam3 or zymosan in the presence or absence of MitoTEMPO, then the release of IFNβ and TNF was quantified by ELISA (Fig. 4F). We observed that while MitoTEMPO had no effect on IFNβ release in TGFβ (−) FLAMs, there was a significant ∼4-fold decrease in IFNβ in MitoTEMPO-treated TGFβ (+) FLAMs activated with both Pam3 and zymosan. In contrast, we observed higher overall levels of TNF release from TGFβ (−) FLAMs compared to TGFβ (+) FLAMs following Pam3 or zymosan activation, but we observed no effect of MitoTEMPO on TNFα release. Taken together, ROS production, likely a result of increased fatty acid metabolism due to elevated peroxisome and mitochondria numbers, appears to be increased in TGFβ (+) FLAMs, resulting in increased mitochondrial oxidative stress following TLR2 activation that contributes to the TGFβ-dependent IFN responses in the TGFβ (+) FLAMs.

Discussion

TGFβ signaling is essential for AM development and homeostasis in the lung environment,[6,14] but how TGFβ signaling regulates the response of AMs to external stimuli remains unclear. Here, we used an ex vivo model of AMs, known as FLAMs, to dissect transcriptional changes in AM-like cells that are mediated by TGFβ. Importantly, our results from this ex vivo FLAM model align with published results from primary AMs in the lungs, suggesting that FLAMs recapitulate many aspects of important biology observed in the lungs.[6] Leveraging this powerful FLAM model, we have now found that while TGFβ restrains a subset of inflammatory pathways, TGFβ primes AMs for mitochondrial oxidative stress and a type I IFN response following treatment with TLR2 agonists. Surprisingly, these TGFβ-regulated, FLAM-specific responses were regulated by MAVS- and IRF3/7-dependent signaling events downstream of TLR2 activation. These results suggest that distinct innate immune signaling networks in AMs are regulated by the tissue environment and directly alter the inflammatory response following the activation of TLR2.

While our findings demonstrate an unexpected link between TLR2, MAVS, and type I IFN production in AMs, the cell biology behind how TLR2 activates type I IFN secretion remains an open question. Several PRRs, including TLR3, TLR7, and TLR9 activate type I IFNs through the activation of IRF3 or IRF7, but these PRRs are localized to the endosome and generally respond to viral ligands.[51,52] In contrast, TLR2 is present on both the surface and in the endosome, similar to TLR4.[53] Previous studies showed that TLR4 signaling through the plasma membrane drives MyD88-dependent NF-κβ activation, while signaling through the endosome activates a TRIF-dependent type I IFN response.[54] Additionally, endosomal TLR2 signaling is necessary for IFNβ production,[55] but the exact signaling adaptors necessary remain controversial, with some reporting roles for TRAM and TRIF[56] and others just TRAM.[57] Whether the localization of TLR2 drives the type I IFN response in TGFβ-cultured FLAMs and how the adaptors MyD88, TRAM, and TRIF contribute to this response will need to be determined. While several previous studies suggest TLR2 can activate type I IFNs, the ligands and cell types capable of this response remain controversial.[55,57–59] For example, Barbalat et al. showed that BMDMs can make type I IFN in response to viral ligands but not bacterial ligands, while Dietrich et al. showed that BMDMs can make type I IFN following activation with bacterial ligands.[55,58] Our data support the role of bacterial and fungal TLR2 ligands in activating a type I IFN response in AMs that is dependent on TGFβ signaling. FLAMs grown in the absence of TGFβ did not robustly induce type I IFNs following TLR2 activation. Our genetic studies found that IRF3, IRF7, and MAVS were all required for the TLR2-dependent type I IFN response. This suggests TLR2-mediated type I IFN may activate parallel pathways, one dependent on direct signaling through MyD88/TRIF, and a second dependent on the cytosolic nucleotide sensing pathways dependent on MAVS. Our data suggest a model where TGFβ primes AMs to enhance the activation of MAVS-dependent type I IFN production.

The mechanisms underlying TGFβ priming of the type I IFN response in AMs remain unknown. TGFβ is known to activate PPARγ and fatty acid oxidation,[6] which we confirmed through our transcriptional analysis. Previous studies have linked

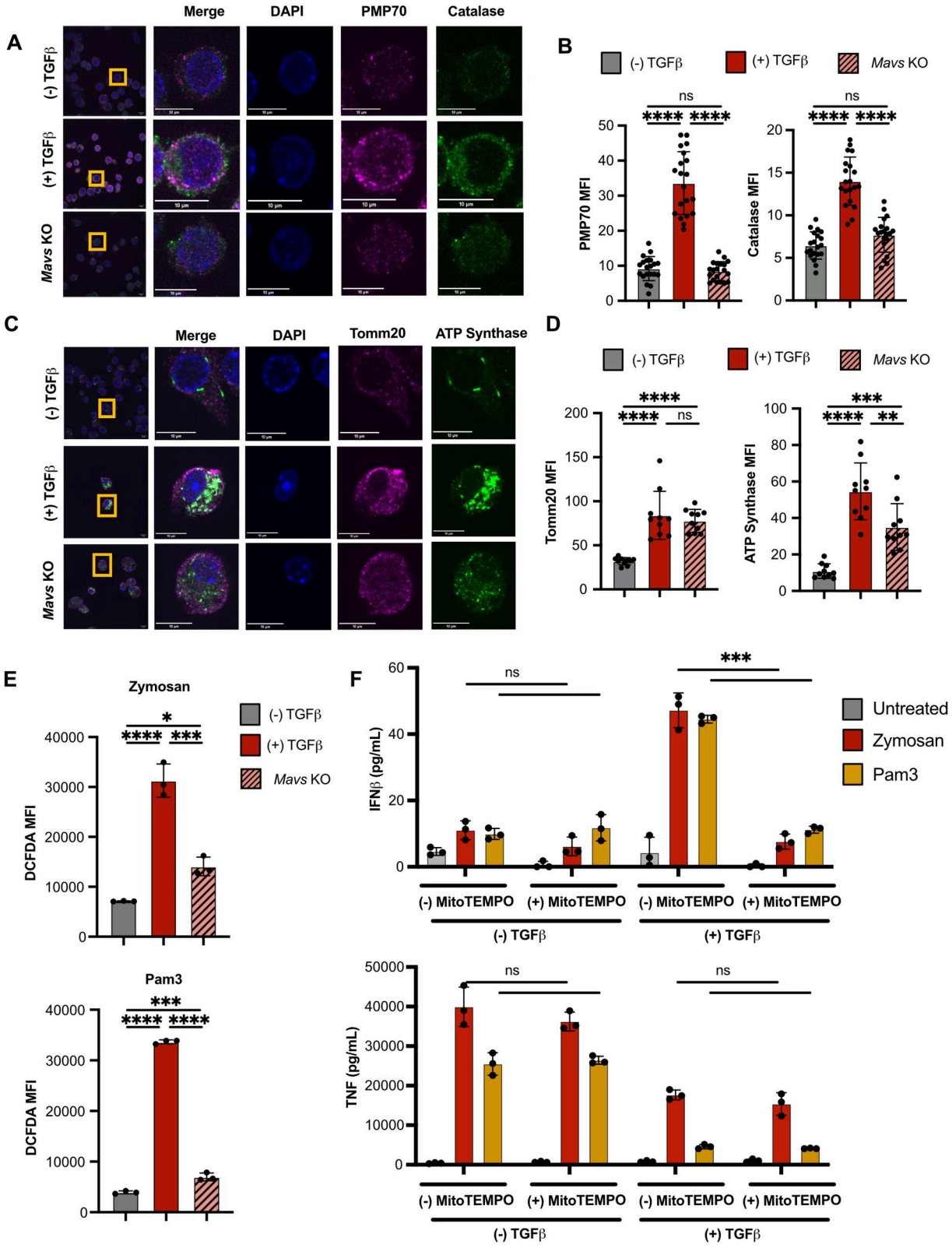

Figure 4. Mitochondrial ROS contributes to TGFβ-dependent IFN responses. (A) WT TGFβ (−) FLAMs and WT or *Mavs* KO TGFβ (+) FLAMs were stained for the peroxisomal markers PMP70 and catalase in addition to cellular DNA with DAPI. Shown are representative images from at least 3 independent experiments. The far-left column images were taken with a 100× oil objective; inset images were cropped to a single cell and have a scale bar that is 10 μm in size. (B) MFI of each peroxisomal marker in (A) was quantified. Each individual data point represents a single cell from a representative experiment. (C) WT TGFβ (−) FLAMs and WT or *Mavs* KO TGFβ (+) FLAMs were stained for the mitochondrial markers Tomm20 and ATP synthase in addition to cellular DNA with DAPI. Shown are representative images from at least 3 independent experiments. The far-left column images were

Figure 4. Continued
taken with a 100× oil objective; inset images were cropped to a single cell and have a scale bar that is 10 μm in size. (D) The MFI of each mitochondrial marker in (C) was quantified. Each individual data point represents a single cell from a representative experiment. (E) WT TGFβ (−) FLAMs and WT or *Mavs* KO TGFβ (+) FLAMs were incubated with DCFDA-H2DCFDA, then left untreated or stimulated with zymosan for 4 h or Pam3 for 1 h followed by flow cytometry analysis. Shown is the MFI for DCFDA-H2DCFDA staining of live cells. Each point represents data from a single well from 1 representative experiment of 2 experiments with Pam3 and 4 experiments with zymosan. (F) WT TGFβ (−) and TGFβ (+) FLAMs were left untreated or activated with zymosan or Pam3 in the presence of absence of MitoTEMPO; 18 h later, secreted IFNβ and TNFα were quantified by ELISA. Each point represents data from a single well from 1 of 4 representative experiments. *$P<0.05$, **$P<0.01$, ***$P<0.001$, ****$P<0.0001$ by 1-way ANOVA with a Tukey post hoc test for multiple comparisons. ns, not significant.

cellular metabolism and type I IFN production. Both cholesterol biosynthesis and glycolysis byproducts, such as lactate, are known to regulate the magnitude of the type I IFN response in BMDMs.[60,61] Our microscopy results and transcriptional analysis showed increased fatty acid oxidation and mitochondrial function in TGFβ (+) FLAMs, which may be upstream drivers of subsequent type I IFN responses following TLR2 activation. Since we observed increased activation of MAVS-dependent type I IFN production following TLR2 stimulation, this suggested the possibility of endogenous cellular ligands such as mitochondrial DNA amplifying the TLR2 response in AMs.[46] Our results with MitoTEMPO further point towards dysfunctional mitochondria as the source of ligands for activating MAVS. Yet more detailed kinetic studies of mitochondrial dynamics and cellular metabolism are warranted, as their contribution to the production of IFNβ remains unknown. Future studies will be needed to dissect the role of fatty acid oxidation, oxidative respiration, and mitochondrial damage in driving TLR2-mediated TGFβ-dependent type I IFN responses in AMs.

Our finding that AMs are uniquely programmed by TGFβ to drive a type I IFN response suggests that these specialized resident macrophages differentially activate their inflammatory profiles in the lung environment compared to other macrophages. In vivo, AMs are known to be important sources of IFNβ following respiratory viral infections with either influenza A virus[62] or respiratory syncytial virus.[63] AMs are known to be sources of type I IFNs following bacterial infection with *Mycobacterium tuberculosis*[64,65] or *Streptococcus pneumoniae.*[66] Following *Aspergillus fumigatus* challenge, peak type I IFN induction occurs within 3 hours postinoculation,[45,67] which is a time when AMs are the major cell population phagocytosing the fungal conidia. However, others have found that TGFβ may inhibit the type I IFN response.[68,69] Interestingly, the cellular source of TGFβ and cytokine signals received in conjunction are critically important in development and priming cues given to lung macrophage. Recently, it was shown that endothelial-derived TGFβ in conjugation with M-CSF signaling is critical for interstitial macrophage differentiation,[70] which is more similar to the BMDM culture conditions used here, potentially explaining our divergent findings. Understanding the consequences of TGFβ signaling in each of these lung-resident macrophage populations and of a type I IFN–skewed response in the airway space is an important line of research for future studies. Type I IFNs are known to be potent regulators of antiviral immunity, suggesting that the host response in the lungs is particularly tuned to respond to invading viral pathogens.[44] However, type I IFNs also play a key role in controlling respiratory fungal pathogens like *Aspergillus fumigatus.*[67] In several disease states, however, including systemic lupus erythematosus and tuberculosis, elevated type I IFNs are associated with worse disease, and blocking type I IFN has been shown to improve clinical outcomes.[71–73] Our data support the role of type I IFNs as a key initial response to invading pathogens in the lungs and more broadly suggests that the balance of type I IFNs can mediate protective or pathologic host responses.

Interestingly, TGFβ is produced in an inactive form by AMs in the lungs and processed into an active form by integrins on lung epithelial cells, which then signal back to AMs to maintain their function in conjunction with GM-CSF.[6,18,19] This interconnected signaling ensures that AMs are properly tuned to the airspace and suggests that the lung environment is an important mediator of the enhanced type I response observed in AMs. A better understanding of the underlying mechanisms driving TGFβ-dependent type I IFNs may enable the development of therapeutics that modulate the balance of type I IFNs more effectively in the lungs to control infections and prevent autoinflammatory diseases.

Acknowledgments

The authors wish to thank Dr. Henry Higgs, Ann Lavanway, Dr. Daniel Mielcarz, Pat Robinson, and Gary Ward for technical support at Dartmouth College.

Author contributions

Conceptualization: S.M.T., A.W.R., J.J.O., A.J.O. Investigation: S.M.T., A.P.M., T.E.V., L.A.M., A.W.R., K.N.C., F.L., C.T., E.C.S. Formal analysis: All authors. Funding acquisition: J.J.O., A.J.O. Supervision: J.J.O., A.J.O. Writing—original draft: S.M.T., J.J.O., A.J.O. Review and editing: All authors.

Sean M. Thomas (Conceptualization [Lead], Formal analysis [Lead], Investigation [Lead], Validation [Equal], Writing—original draft [Lead], Writing—review & editing [Equal]), Abigail P. McGee (Formal analysis [Equal], Investigation [Equal], Validation [Equal], Writing—review & editing [Equal]), Taryn E. Vielma (Data curation [Equal], Formal analysis [Equal], Investigation [Equal], Writing—review & editing [Equal]), Laurisa M. Ankley (Data curation [Equal], Formal analysis [Equal], Investigation [Equal], Writing—review & editing [Equal]), Alexander W. Rapp (Conceptualization [Equal], Data curation [Equal], Formal analysis [Equal], Investigation [Equal], Writing—review & editing [Equal]), Kayla N. Conner (Data curation [Equal], Formal analysis [Equal], Visualization [Equal], Writing—review & editing [Equal]), Francois LeSage (Formal analysis [Equal], Investigation [Equal], Writing—review & editing [Equal]), Christopher Tanner (Formal analysis [Equal], Investigation [Equal],

Writing—review & editing [Equal]), Eleanor C. Scheeres (Formal analysis [Equal], Investigation [Equal], Writing—review & editing [Equal]), Joshua J. Obar (Conceptualization [Lead], Formal analysis [Lead], Funding acquisition [Lead], Project administration [Lead], Supervision [Lead], Writing—original draft [Lead], Writing—review & editing [Lead]), and Andrew J. Olive (Conceptualization [Lead], Formal analysis [Lead], Funding acquisition [Lead], Project administration [Lead], Supervision [Lead], Writing—original draft [Lead], Writing—review & editing [Lead])

Supplementary material

Supplementary material is available at *The Journal of Immunology* online.

Funding

This work was supported by grants from the National Institutes of Health (NIH): R01 AI139133 (J.J.O) and R35 GM146795 (A.J.O.). A.W.R. was supported by the Dartmouth College Molecular Microbiology and Pathogenesis Program (NIH/National Institute of Allergy and Infectious Diseases [NIAID] T32 AI007519). A.P.M. was supported by the Dartmouth College Immunology Training Program (NIH/NIAID T32 AI007363). F.L. was supported by the Dartmouth College Cystic Fibrosis Training Program (NIH/NIAID T32 HL134598) and CFRDP Training Core from the Cystic Fibrosis Foundation. The Attune CytPix, located in the MSU Flow Cytometry Core Facility, is supported by the Equipment Grants Program, award no. 2022-70410-38419, from the US Department of Agriculture, National Institute of Food and Agriculture. DartLab, the Immune Monitoring and Flow Cytometry Shared Resource at the Dartmouth Cancer Center, is partially supported with National Cancer Institute (NCI) Cancer Center Support Grant 5P30 CA023108-41. The Light Microscopy Facility at Dartmouth is partially supported by bioMT through NIH grant P20-GM113132, DartCF through NIH grant P30-DK117469, and by the Dartmouth Cancer Center through NCI Cancer Center Support Grant P30 CA023108. The purchase of the Nikon SoRa Spinning Disk Confocal Microscope was supported through NIH award S10 OD032310 to Dr. Yashi Ahmed (Dartmouth College).

Conflicts of interest

None declared.

Data availability

All data are available in the manuscript, or through linked online databases with analyzed and raw datasets. RNAseq data is deposited in the National Center for Biotechnology Information's Gene Expression Omnibus database (accession no. GSE276577). Analyzed data in Table S1 are available on Figshare (https://doi.org/10.6084/m9.figshare.28914437).

References

1. Hsia CC, Hyde DM, Weibel ER. Lung structure and the intrinsic challenges of gas exchange. Compr Physiol. 2016;6:827–895.
2. Kopf M, Schneider C, Nobs SP. The development and function of lung-resident macrophages and dendritic cells. Nat Immunol. 2015;16:36–44.
3. Branchett WJ, Lloyd CM. Regulatory cytokine function in the respiratory tract. Mucosal Immunol. 2019;12:589–600.
4. Wu Y, Hirschi KK. Tissue-resident macrophage development and function. Front Cell Dev Biol. 2020;8:617879.
5. van de Laar L et al. Yolk sac macrophages, fetal liver, and adult monocytes can colonize an empty niche and develop into functional tissue-resident macrophages. Immunity. 2016;44:755–768.
6. Yu X et al. The cytokine TGF-β promotes the development and homeostasis of alveolar macrophages. Immunity. 2017;47:903–912.e4.
7. Ardain A, Marakalala MJ, Leslie A. Tissue-resident innate immunity in the lung. Immunology. 2020;159:245–256.
8. Rothchild AC et al. Alveolar macrophages generate a noncanonical NRF2-driven transcriptional response to *Mycobacterium tuberculosis* in vivo. Sci Immunol. 2019;4:eaaw6693.
9. Pisu D, Huang L, Grenier JK, Russell DG. Dual RNA-seq of Mtb-infected macrophages in vivo reveals ontologically distinct host-pathogen interactions. Cell Rep. 2020;30:335–350.e4.
10. Huang L, Nazarova EV, Tan S, Liu Y, Russell DG. Growth of *Mycobacterium tuberculosis* in vivo segregates with host macrophage metabolism and ontogeny. J Exp Med. 2018;215:1135–1152.
11. Aegerter H et al. Influenza-induced monocyte-derived alveolar macrophages confer prolonged antibacterial protection. Nat Immunol. 2020;21:145–157.
12. Suzuki T et al. Familial pulmonary alveolar proteinosis caused by mutations in CSF2RA. J Exp Med. 2008;205:2703–2710.
13. Schneider C et al. Induction of the nuclear receptor PPAR-γ by the cytokine GM-CSF is critical for the differentiation of fetal monocytes into alveolar macrophages. Nat Immunol. 2014;15:1026–1037.
14. Branchett WJ et al. Airway macrophage-intrinsic TGF-β1 regulates pulmonary immunity during early-life allergen exposure. J Allergy Clin Immunol. 2021;147:1892–1906.
15. Tzavlaki K, Moustakas A. TGF-beta signaling. Biomolecules. 2020;10:487.
16. Nunes I, Shapiro RL, Rifkin DB. Characterization of latent TGF-beta activation by murine peritoneal macrophages. J Immunol. 1995;155:1450–1459.
17. Dennis PA, Rifkin DB. Cellular activation of latent transforming growth factor beta requires binding to the cation-independent mannose 6-phosphate/insulin-like growth factor type II receptor. Proc Natl Acad Sci U S A. 1991;88:580–584.
18. Annes JP, Rifkin DB, Munger JS. The integrin alphaVbeta6 binds and activates latent TGFbeta3. FEBS Lett. 2002;511:65–68.
19. Gleizes PE et al. TGF-beta latency: biological significance and mechanisms of activation. Stem Cells. 1997;15:190–197.
20. Gong D et al. TGFβ signaling plays a critical role in promoting alternative macrophage activation. BMC Immunol. 2012;13:31.

21. Gratchev A. TGF-β signalling in tumour associated macrophages. Immunobiology. 2017;222:75–81.
22. Chung JY et al. TGF-β signaling: from tissue fibrosis to tumor microenvironment. Int J Mol Sci. 2021;22:7575.
23. Chen H et al. TGF-β receptor II in epithelia versus mesenchyme plays distinct roles in the developing lung. Eur Respir J. 2008;32:285–295.
24. Sanford LP et al. TGFβ2 knockout mice have multiple developmental defects that are non-overlapping with other TGFβ knockout phenotypes. Development. 1997;124:2659–2670.
25. Kulkarni AB et al. Transforming growth factor beta 1 null mutation in mice causes excessive inflammatory response and early death. Proc Natl Acad Sci U S A. 1993;90:770–774.
26. Shull MM et al. Targeted disruption of the mouse transforming growth factor-beta 1 gene results in multifocal inflammatory disease. Nature. 1992;359:693–699.
27. Willis BC et al. Induction of epithelial-mesenchymal transition in alveolar epithelial cells by transforming growth factor-beta1: potential role in idiopathic pulmonary fibrosis. Am J Pathol. 2005;166:1321–1332.
28. Frangogiannis N. Transforming growth factor-β in tissue fibrosis. J Exp Med. 2020;217:e20190103.
29. Garrison G et al. Reversal of myofibroblast differentiation by prostaglandin E(2). Am J Respir Cell Mol Biol. 2013; 48:550–558.
30. Gorki AD et al. Murine ex vivo cultured alveolar macrophages provide a novel tool to study tissue-resident macrophage behavior and function. Am J Respir Cell Mol Biol. 2022; 66:64–75.
31. Luo M, Lai W, He Z, Wu L. Development of an optimized culture system for generating mouse alveolar macrophage-like cells. J Immunol. 2021;207:1683–1693.
32. Thomas ST, Wierenga KA, Pestka JJ, Olive AJ. Fetal liver-derived alveolar-like macrophages: a self-replicating ex vivo model of alveolar macrophages for functional genetic studies. Immunohorizons. 2022;6:156–169.
33. Smith MR, Standiford TJ, Reddy RC. PPARs in alveolar macrophage biology. PPAR Res. 2007;2007:23812.
34. Baker AD et al. Targeted PPARγ deficiency in alveolar macrophages disrupts surfactant catabolism. J Lipid Res. 2010; 51:1325–1331.
35. Remmerie A, Scott CL. Macrophages and lipid metabolism. Cell Immunol. 2018;330:27–42.
36. Heng TS, Painter MW; Immunological Genome Project Consortium. The immunological genome project: networks of gene expression in immune cells. Nat Immunol. 2008; 9:1091–1094.
37. Oliveira-Nascimento L, Massari P, Wetzler LM. The role of TLR2 in infection and immunity. Front Immunol. 2012;3:79.
38. Gopalakrishnan A, Salgame P. Toll-like receptor 2 in host defense against Mycobacterium tuberculosis: to be or not to be—that is the question. Curr Opin Immunol. 2016;42:76–82.
39. Rubino I et al. Species-specific recognition of *Aspergillus fumigatus* by Toll-like receptor 1 and Toll-like receptor 6. J Infect Dis. 2012;205:944–954.
40. Buckland KF, O'Connor E, Murray LA, Hogaboam CM. Toll like receptor-2 modulates both innate and adaptive immune responses during chronic fungal asthma in mice. Inflamm Res. 2008;57:379–387.
41. Balloy V et al. Involvement of toll-like receptor 2 in experimental invasive pulmonary aspergillosis. Infect Immun. 2005;73:5420–5425.
42. Goodridge HS, Wolf AJ, Underhill DM. Beta-glucan recognition by the innate immune system. Immunol Rev. 2009; 230:38–50.
43. Ivashkiv LB, Donlin LT. Regulation of type I interferon responses. Nat Rev Immunol. 2014;14:36–49.
44. McNab F, Mayer-Barber K, Sher A, Wack A, O'Garra A. Type I interferons in infectious disease. Nat Rev Immunol. 2015; 15:87–103.
45. Wang X et al. MDA5 is an essential sensor of a pathogen-associated molecular pattern associated with vitality that is necessary for host resistance against *Aspergillus fumigatus*. J Immunol. 2020;205:3058–3070.
46. West AP, Shadel GS. Mitochondrial DNA in innate immune responses and inflammatory pathology. Nat Rev Immunol. 2017;17:363–375.
47. Dixit E et al. Peroxisomes are signaling platforms for antiviral innate immunity. Cell. 2010;141:668–681.
48. Koenig A, Buskiewicz-Koenig IA. Redox activation of mitochondrial DAMPs and the metabolic consequences for development of autoimmunity. Antioxid Redox Signal. 2022;36: 441–461.
49. Buskiewicz IA et al. Reactive oxygen species induce virus-independent MAVS oligomerization in systemic lupus erythematosus. Sci Signal. 2016;9:ra115.
50. Trnka J, Blaikie FH, Smith RA, Murphy MP. A mitochondria-targeted nitroxide is reduced to its hydroxylamine by ubiquinol in mitochondria. Free Radic Biol Med. 2008;44:1406–1419.
51. Thompson MR, Kaminski JJ, Kurt-Jones EA, Fitzgerald KA. Pattern recognition receptors and the innate immune response to viral infection. Viruses. 2011;3:920–940.
52. Li D, Wu M. Pattern recognition receptors in health and diseases. Signal Transduct Target Ther. 2021;6:291.
53. Kawai T, Akira S. Toll-like receptors and their crosstalk with other innate receptors in infection and immunity. Immunity. 2011;34:637–650.
54. Toshchakov V et al. TLR4, but not TLR2, mediates IFN-beta-induced STAT1alpha/beta-dependent gene expression in macrophages. Nat Immunol. 2002;3:392–398.
55. Dietrich N, Lienenklaus S, Weiss S, Gekara NO. Murine Toll-like receptor 2 activation induces type I interferon responses from endolysosomal compartments. PLoS One. 2010;5: e10250.
56. Nilsen NJ et al. A role for the adaptor proteins TRAM and TRIF in Toll-like receptor 2 signaling. J Biol Chem. 2015; 290:3209–3222.
57. Stack J et al. TRAM is required for TLR2 endosomal signaling to type I IFN induction. J Immunol. 2014;193:6090–6102.
58. Barbalat R, Lau L, Locksley RM, Barton GM. Toll-like receptor 2 on inflammatory monocytes induces type I interferon in response to viral but not bacterial ligands. Nat Immunol. 2009; 10:1200–1207.
59. Oosenbrug T, van de Graaff MJ, Haks MC, van Kasteren S, Ressing ME. An alternative model for type I interferon induction downstream of human TLR2. J Biol Chem. 2020;295: 14325–14342.

60. York AG et al. Limiting cholesterol biosynthetic flux spontaneously engages type I IFN signaling. Cell. 2015;163:1716–1729.
61. Zhang W et al. Lactate is a natural suppressor of RLR signaling by targeting MAVS. Cell. 2019;178:176–189.e15.
62. Hogner K et al. Correction: macrophage-expressed IFN-β contributes to apoptotic alveolar epithelial cell injury in severe influenza virus pneumonia. PLoS Pathog. 2016;12:e1005716.
63. Goritzka M et al. Alveolar macrophage-derived type I interferons orchestrate innate immunity to RSV through recruitment of antiviral monocytes. J Exp Med. 2015;212:699–714.
64. Branchett WJ et al. Type I IFN drives neutrophil swarming, impeding lung T cell-macrophage interactions and TB control. J Exp Med. 2025;222:e20250466.
65. Sadee W et al. Human alveolar macrophage response to *Mycobacterium tuberculosis*: immune characteristics underlying large inter-individual variability. Commun Biol. 2025;8:950.
66. Maier BB et al. Type I interferon promotes alveolar epithelial type II cell survival during pulmonary *Streptococcus pneumoniae* infection and sterile lung injury in mice. Eur J Immunol. 2016;46:2175–2186.
67. Espinosa V et al. Type III interferon is a critical regulator of innate antifungal immunity. Sci Immunol. 2017;2:eaan5357.
68. Grunwell JR et al. TGF-β1 suppresses the type I IFN response and induces mitochondrial dysfunction in alveolar macrophages. J Immunol. 2018;200:2115–2128.
69. Meliopoulos VA et al. An epithelial integrin regulates the amplitude of protective lung interferon responses against multiple respiratory pathogens. PLoS Pathog. 2016;12:e1005804.
70. Peng W et al. Endothelial-driven TGFβ signaling supports lung interstitial macrophage development from monocytes. Sci Immunol. 2025;10:eadr4977.
71. Mayer-Barber KD et al. Host-directed therapy of tuberculosis based on interleukin-1 and type I interferon crosstalk. Nature. 2014;511:99–103.
72. Ji DX et al. Role of the transcriptional regulator SP140 in resistance to bacterial infections via repression of type I interferons. Elife. 2021;10:e67290.
73. Postal M et al. Type I interferon in the pathogenesis of systemic lupus erythematosus. Curr Opin Immunol. 2020;67:87–94.
74. Tighe RM, Birukova A, Yaeger MJ, Reece SW, Gowdy KM. Euthanasia- and lavage-mediated effects on bronchoalveolar measures of lung injury and inflammation. Am J Respir Cell Mol Biol. 2018;59:257–266.
75. Fulco CP et al. Systematic mapping of functional enhancer-promoter connections with CRISPR interference. Science. 2016;354:769–773.
76. Shalem O et al. Genome-scale CRISPR-Cas9 knockout screening in human cells. Science. 2014;343:84–87.
77. Conant D et al. Inference of CRISPR edits from sanger trace data. CRISPR J. 2022;5:123–130.
78. Langmead B, Salzberg SL. Fast gapped-read alignment with Bowtie 2. Nat Methods. 2012;9:357–359.
79. Liao Y, Smyth GK, Shi W. featureCounts: an efficient general purpose program for assigning sequence reads to genomic features. Bioinformatics. 2014;30:923–930.
80. Love MI, Huber W, Anders S. Moderated estimation of fold change and dispersion for RNA-seq data with DESeq2. Genome Biol. 2014;15:550.

The Journal of Immunology, 2026, 215, 1–15
https://doi.org/10.1093/jimmun/vkag090
Cutting Edge